

Exploiting Task Relationships for Continual Learning Using Transferability-Aware Task Embeddings

Yanru Wu¹ Xiangyu Chen¹ Jianning Wang² Enming Zhang¹ Hanbing Liu¹ Yang Li^{*1}

* Corresponding author

¹Shenzhen Key Laboratory of Ubiquitous Data Enabling, Shenzhen International Graduate School, Tsinghua University

²Independent Researcher

Abstract

Continual learning (CL) has been an essential topic in the contemporary application of deep neural networks, where catastrophic forgetting (CF) can impede a model’s ability to acquire knowledge progressively. Existing CL strategies primarily address CF by regularizing model updates or separating task-specific and shared components. However, these methods focus on task model elements while overlooking the potential of leveraging inter-task relationships for learning enhancement. To address this, we propose a transferability-aware task embedding named H-embedding and train a hypernet under its guidance to learn task-conditioned model weights for CL tasks. Particularly, H-embedding is introduced based on an information theoretical transferability measure and is designed to be online and easy to compute. The framework is also characterized by notable practicality, which only requires storing a low-dimensional task embedding for each task, and can be efficiently trained in an end-to-end way. Extensive evaluations and experimental analyses on datasets including Permuted MNIST, Cifar10/100, and ImageNet-R demonstrate that our framework performs prominently compared to various baseline methods, displaying great potential in exploiting intrinsic task relationships.

1 INTRODUCTION

Continual learning (CL), also known as incremental learning or life-long learning, has been an important topic in the modern application of deep neural networks, where a model is expected to learn a series of tasks sequentially for the optimization of its capability [Wang et al., 2024]. However, in practical usage, catastrophic forgetting (CF) [Kirkpatrick et al., 2017] can hamper the model from cumulatively gain-

ing knowledge as intended, severely hindering the overall growth of model capacity and resulting in significant waste of training resources. Specifically, in CL settings, a model is trained one-by-one (*i.e.*, data in the old tasks are not fully available anymore when training new ones) on a sequence of tasks, which typically contains either category change or data distribution shifts [Qu et al., 2021]. Consider the training process of a new task, a desirable model performance should be characterized by two aspects (depicted in Fig. 1) [von Oswald et al., 2020]. 1) **Backward Transfer / Non-Catastrophic Forgetting** [Kirkpatrick et al., 2017]: improvement or at least no significant degradation on previous tasks. 2) **Forward Transfer**: higher efficiency in learning the new task compared to training a model from scratch.

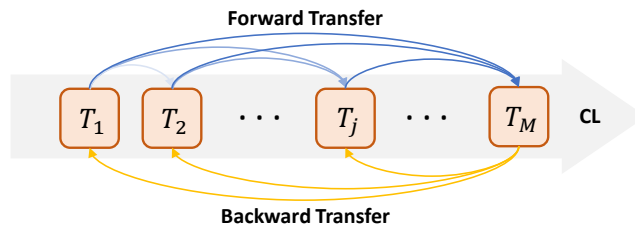


Figure 1: **Illustration of backward and forward transfer during CL.** $\{T_j\}_{j=1}^M$ denotes the CL tasks.

Up to now, there have been many studies dedicated to CL strategies, most of them involving the rehearsal of previous data to alleviate the knowledge degradation caused by CF. However, growing concerns about privacy and data safety have made this solution not always feasible, bringing increased attention to the *rehearsal-free* CL setting Smith et al. [2023]. Previous works on rehearsal-free CL can be mostly described as regularization-based approaches, including parameter space regularization [e.g. Kirkpatrick et al., 2017, Zenke et al., 2017] and feature space regularization [e.g. Li and Hoiem, 2017, Rebuffi et al., 2017]. These approaches introduce different regularization losses during training on the model weights, the intermediate layer, or the final output. Despite their effectiveness, regularization methods are lim-

ited in their design that the models learned on subsequent tasks are forced to stay close to those on previous tasks, while in fact the tasks in a CL setting are not necessarily similar to each other. On the other hand, architecture-based approaches [Wang et al., 2024] emerge as an alternative solution¹. Rather than attempting to forcibly align all tasks in their model parameters or outputs, they generally aim at dedicating task-specific and task-sharing model components from different architecture levels [e.g. Mallya and Lazebnik, 2018, Wortsman et al., 2020, Jin and Kim, 2022], and tailoring the training process accordingly. Nevertheless, the allocation of model parts to different tasks usually comes with scaling problems with the growth of task numbers, potentially resulting in insufficient model capacity or excessive model size growth.

These bring us to a fundamental question in continual learning: *Positive backward and forward transfers in CL rely on capturing the underlying relationship between different tasks, but how do we efficiently learn and utilize such relations as we train the model?* Previous works primarily focus on model elements, either by regularizing model updates or by distinguishing task-specific and task-sharing components. Although effective in mitigating CF, these approaches are largely constrained by a trade-off between forward and backward transfer, overlooking the potential of better exploiting task relationships for an overall learning improvement. This oversight often leads to inadequate CF mitigation or limited forward transfer performance, where the incorporation of prior knowledge on task relationships through statistical tools would substantially benefit CL performance.

Therefore, recognizing the shared goal between identifying prior relationships among tasks and the role of transferability metrics [Ding et al., 2024] in evaluating source-target task compatibility, we propose in this work a CL framework guided by transferability-based task embeddings. Specifically, we introduce an online task embedding scheme named H-embedding, which distills the transferability information into a low-dimensional embedding through an optimization process. H-embedding can be learned efficiently without accessing previous data by maximizing the consistency between the Euclidean distance of embeddings and the H-score [Bao et al., 2019] transferability among the corresponding tasks. To match the property of embedding distances with transferability scores, we further apply analytic hierarchy process (AHP) normalization to the transferability values, significantly improving learning stability over long task sequences without compromising efficiency. Building on this, we present a hypernet-based CL framework, where a task-conditioned hypernetwork [von Oswald et al., 2020, more in Sec. 2] is trained to generate task-specific model weights based on H-embedding modulated task embeddings.

¹A large proportion of these approaches actually require certain access to previous data and do not conform to rehearsal-free setting. We cover them here mainly for discussion comprehensiveness.

In summary, with the aim of better understanding and utilization of the task space in CL, we propose in this work a novel H-embedding guided hypernet framework. Our framework is featured by: 1) efficient and reliable learning of task embedding based on the information theoretical foundation of H-score metric; 2) a notable enhancement of CL in the overall performance; 3) ease of practical use with end-to-end training and minimal additional storage beyond low-dimensional task embeddings.

2 RELATED WORKS

2.1 REHEARSAL-FREE CONTINUAL LEARNING

The strictness of CL settings varies with the extent of allowed previous data accessibility. Multi-task learning [Caruana, 1997], with full data availability of all tasks, can actually be viewed as a special case of CL, while rehearsal-free CL [Smith et al., 2023], with no previous data involved in the training of new tasks, is the strictest CL setting under this criteria. Despite the success of rehearsal-based methods in various benchmarks [Bang et al., 2021, Shin et al., 2017, Belouadah and Popescu, 2019], rehearsal-free CL is catching the attention of researchers recently [Smith et al., 2023] because of its low dependency on revisiting previous tasks and therefore broader application in the era of growing data privacy concern. Existing works on rehearsal-free CL are mostly based on regularization strategies. EWC [Kirkpatrick et al., 2017] and SI [Zenke et al., 2017] introduce penalties to restrict the alteration of parameters vital for addressing prior tasks, thereby reducing the risk of CF. LwF [Li and Hoiem, 2017, Rebuffi et al., 2017] proposes a cross-entropy loss between the predicted class distribution of the $(n-1)$ -th task, as generated by the model before and after learning the n -th task. Smith et al. [2023] reviews these methods and proposes regularization combinations for better CL performance. In this work, we follow these works and focus on the more challenging rehearsal-free CL setting.

2.2 HYPERNETS

Hypernets [Ha et al., 2017], or hypernetworks, are specialized neural networks that produce weights for another neural network, *i.e.*, the target network. Recently, they have gained recognition as a potent tool in deep learning, providing advantages such as increased flexibility, adaptability, dynamic nature, training efficiency, and model compression [Chauhan et al., 2023]. Hypernets have yielded encouraging results in various deep learning applications, including continual learning [von Oswald et al., 2020], causal inference [Chauhan et al., 2024], domain adaptation [Volk et al., 2022], uncertainty quantification [Krueger et al., 2017], few-shot learning [Sendra et al., 2023], and reinforcement learning [Sarafian et al., 2021].

2.3 TRANSFERABILITY METRICS

Task transferability [Zamir et al., 2018] investigates the relationships between tasks and provides an effective method to evaluate and select source tasks in transfer learning. It also plays a crucial role in developing strategies for multi-task learning and meta-learning. For ease of use, previous studies have proposed metrics based on task models and data distributions for a quick estimation of transferability [Ding et al., 2024]. H-score [Bao et al., 2019, Ibrahim et al., 2022, Wu et al., 2024] uses an information-theoretic framework to evaluate transferability by solving a maximum correlation problem. NCE [Tran et al., 2019] employs conditional entropy to assess transferability and task difficulty. LEEP score [Nguyen et al., 2020, Agostinelli et al., 2022] offers a more generalized metric, defined by measuring the performance of a classifier developed from source model predictions when applied to the target task. LogME [You et al., 2021] assesses target task accuracy using a formulation integrating all possible linear classifiers derived from source model features. OTCE [Tan et al., 2021, 2024] combines optimal transport with conditional entropy to both estimate the domain and task difference between source and target. These metrics are mostly designed with differed assumptions and source accessibility, with their use applicable to different problem settings.

3 PRELIMINARY

3.1 MATHEMATICAL FORMULATION

Consider a problem setting consisting of M tasks $\{T_j\}_{j=1}^M$, the data of task j is denoted by $D_j = (X^{(j)}, Y^{(j)})$, with input samples $X^{(j)} = \{x^{(j,i)}\}_{i=1}^{N_j}$ and output samples $Y^{(j)} = \{y^{(j,i)}\}_{i=1}^{N_j}$. Here, $N_j = |X^{(j)}| = |Y^{(j)}|$ denotes the sample size of the j -th task, and the attributes of sample data $x^{(j,i)}, y^{(j,i)}$ depends on the particular CL setting as well as the form of tasks. In CL, the M tasks are learned sequentially during the training stage. To be specific, denoting a neural network model as $f(x, \Theta)$ (where f represents the model function, x represents the input data, and Θ represents the model weights) and the model weights acquired in task $j - 1$ as $\Theta^{(j-1)}$, the goal of learning task j is to derive a new set of weights $\Theta^{(j)}$ that not only achieves the optimal performance on task j , but also performs better or not significantly worse than $\Theta^{(j-1)}$ on tasks T_1, \dots, T_{j-1} . For a rehearsal-free CL setting, the previous data D_1, \dots, D_{j-1} are not accessible during the training of the j -th task.

3.2 H-SCORE

H-score is firstly introduced by Huang et al. in 2019 as a metric assessing the informativeness of features for a task. Theoretically derived from the maximal correlation

interpretation of deep neural networks, its mathematical foundation roots to the information theory work known as maximal correlation analysis, which originates from the works of Hirschfeld, Gebelein and Renyi [Hirschfeld, 1935, Gebelein, 1941, Rényi, 1959] and has been followed and further explored by a broad spectrum of successive work. The H-score of f with regard to the task casting X to Y is defined as:

$$H(f) = \text{tr}(\text{cov}(f(X))^{-1} \text{cov}(\mathbb{E}_{P_{X|Y}}[f(X)|Y])), \quad (1)$$

with input data X , label Y and feature extractor function $f(X)$. Subsequent work has extended H-score to also serve as a metric for transferability and validated its efficiency with extensive experiments [Bao et al., 2019, Ibrahim et al., 2022], implying the potential of H-score for transfer learning and its application in related problems. The choice of H-score employment in our framework is because of its strong theoretical reliability, conformity of assumption to our problem setting, as well as its non-dependence on source data which makes possible an online embedding estimation.

4 METHODOLOGY

4.1 HYPERNET-BASED CL FRAMEWORK

Unlike most existing approaches that are limited to the exploration of model elements, in this work we propose a hypernet-based CL framework to maximally leverage knowledge about task relationships for task model generation.

Following von Oswald et al. [2020]², a task-conditioned hypernetwork $f_h(e, \Theta_h)$ with hypernet weights Θ_h is introduced to map a task embedding e to the corresponding model weights Θ of task model f . On this basis, we present a framework (illustrated in Fig. 2) that guides the hypernet with the transferability-based H-embedding \hat{e} . Specifically, all tasks $\{T_j\}_{j=1}^M$ in the learning scenario share a single hypernet f_h that generates their task model weights using their task-specific embeddings $\{e^{(j)}\}_{j=1}^M$, i.e. $\Theta^{(j)} = f_h(e^{(j)}, \Theta_h)$ for task j . When learning each task T_j , the task embedding $e^{(j)}$ is simultaneously updated with the training of hypernet parameters Θ_h , while parameters other than Θ_h and $e^{(j)}$ are fixed and can be viewed as constants. The learning of $e^{(j)}$ and Θ_h is regularized using previous task embeddings $\{e^{(n)}\}_{n=1}^{j-1}$ and H-embedding $\hat{e}^{(j)}$ to ensure backward and forward transfer performance. The learning loss is composed of three parts:

- Target loss, a supervised loss to learn current task j .

$$\begin{aligned} \mathcal{L}_t &= \mathcal{L}(f(x^{(j)}, \Theta^{(j)}), y^{(j)}) \\ &= \mathcal{L}(f(x^{(j)}, f_h(e^{(j)}, \Theta_h)), y^{(j)}) \end{aligned} \quad (2)$$

²In fact, this guidance is more general and can be incorporated into any hypernet-based CL framework, yet here we mainly base our framework on the work of von Oswald et al. [2020].

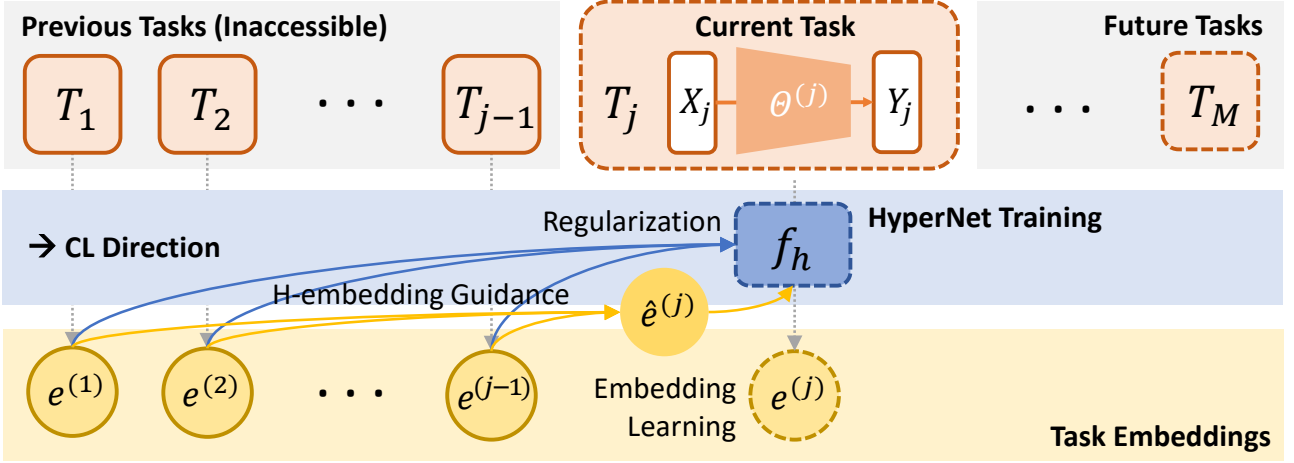


Figure 2: **Illustration of the CL status on the step of learning task j under our framework.** The hypernet is being trained to provide the optimal task model weight $\Theta^{(j)}$ concurrently with the learning of current task embedding $e^{(j)}$, where regularization and guidance are applied using previous embeddings and H-embeddings.

- Continual learning loss (same as introduced by von Oswald et al. [2020]), to prevent CF by ensuring that given previous task embeddings $\{e^{(n)}\}_{n=1}^{j-1}$, the network weights output by the hypernet before and after training on task j are analogous.

$$\begin{aligned}
 L_c &= \frac{1}{j-1} \sum_{n=1}^{j-1} L_c^{(n)} \\
 &= \frac{1}{j-1} \sum_{n=1}^{j-1} \|f_h(e^{(n)}, \Theta_h) - f_h(e^{(n)}, \Theta_h^*)\|^2
 \end{aligned} \quad (3)$$

- H-embedding guidance loss, to provide the hypernet with additional prior knowledge about the task relationships using transferability.

$$L_e = L_e(e^{(j)}, \hat{e}^{(j)}) \quad (4)$$

Here, \mathcal{L} denotes certain supervised task loss (cross-entropy loss in our experiments), and Θ_h^* is the set of hypernet parameters before learning task j . The definition of the embedding regularization loss L_e will be covered in later sections. To summarize, our final loss function is as follows with hyperparameters β_e and β_c :

$$L = L_t + \beta_e L_e + \beta_c L_c \quad (5)$$

On the j -th task, our approach for the training of T_j is depicted in Fig. 3. Notably, although it may appear that the task model weights are first generated and subsequently used for inference, the framework is actually end-to-end, with the hypernet parameters Θ_h and embeddings $e^{(j)}$ optimized directly by feeding the task data and minimizing the total loss. Hence, there is no additional training procedure

introduced in our framework, and the only information to save is the low-dimensional³ task embedding $e^{(j)}$.

4.2 H-EMBEDDING GUIDANCE

4.2.1 H-embedding

Building on the desiderata outlined in Sec.1, we incorporate task relationships from accessible data into a prior embedding to guide the CL framework. Specifically, we propose an H-score-based online task embedding, named H-embedding.

During the training stage of task j , we first measure the H-score transferability from each previous task $\{T_n\}_{n=1}^{j-1}$ to T_j using D_j and previous task embeddings $\{e^{(n)}\}_{n=1}^{j-1}$.

$$\begin{aligned}
 H(T_n, T_j) &= \text{tr}(\text{cov}(f_l(x^{(j)}, \Theta^{(n)}))^{-1} \\
 &\quad \text{cov}(\mathbb{E}_{P_{X|Y}}[f_l(x^{(j)}, \Theta^{(n)})|y^{(j)}])) \\
 \Theta^{(n)} &= f_h(e^{(n)}, \Theta_h)
 \end{aligned} \quad (6)$$

Here, we leverage the convenience that previous task models can be reconstructed by the hypernet and corresponding task embeddings. $f_l(\ast)$ denotes the output of the last hidden layer in the task model f , which can be viewed as the feature of task data $X^{(j)}$. The H-embedding $\hat{e}^{(j)}$ is then computed by minimizing the difference between the Euclidean distance of $e^{(n)}$, $\hat{e}^{(j)}$ and their reversed H-score transferability $H(T_n, T_j)$:

$$\hat{e}^{(j)} = \arg \min_{\hat{e}^{(j)}} \sum_{n=1}^{j-1} \left(\|\hat{e}^{(j)} - e^{(n)}\|_2 - 1/H(T_n, T_j) \right)^2, \quad (7)$$

³The dimension of task embedding is set to 32 in Cifar10/100 & ImageNet-R and 24 in MNIST experiments.

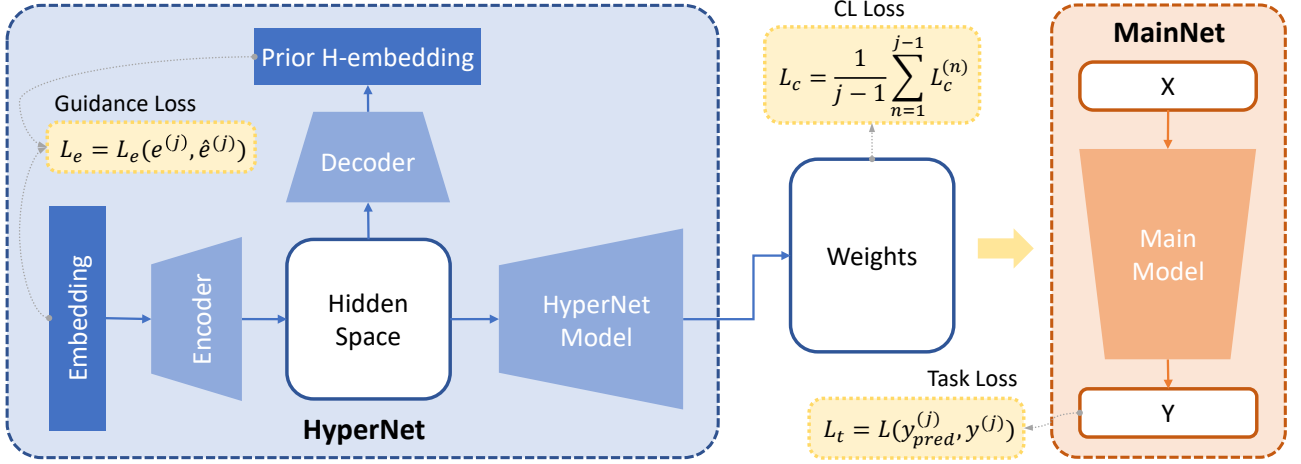


Figure 3: **Framework of our hypernet on the slice of task j .** A hypernet (left, blue) is utilized to learn the weights of the main model (right, orange), where the H-embedding guidance is introduced using an encoder-decoder module. The entire framework is trained end-to-end by inputting task data into the main model and propagating gradients backward to update both hypernet and embedding.

where $e^{(n)}$ is calculated and stored when learning previous tasks. Given that transferability can only be assessed with a minimum of two tasks, H-embeddings and the guidance loss are computed only after completing the first two tasks.

Nevertheless, due to its target-centered intrinsicality, the simple reversal of H-score may not align in property (*i.e.* symmetry and scale) with the Euclidean distance of embeddings learned sequentially on the tasks in CL. Hence, we introduce Analytic Hierarchy Process (AHP) normalization [Zamir et al., 2018] to process the H-score in Eqn. 7. Specifically, we construct a pairwise tournament matrix $W^{(j)} \in \mathbb{R}^{j \times j}$ for task j , with elements given by:

$$w_{m,n}^{(j)} = \frac{H(T_m, T_j)}{H(T_n, T_j)} \quad \forall m, n \in \{1, 2, \dots, j\}, \quad (8)$$

measuring how much times better task m is compared to task n when transferring to task j . Here, we define the self-transferability $H(T_j, T_j)$ as the HGR maximal correlation between X_j and Y_j , with the consistency of transferability definition verified by the theoretical framework of H-score⁴. Consequently, the AHP normalized transferabilities are given by elements of the principal eigenvector $\mathbf{v}^{(j)}$ of $W^{(j)}$, *i.e.* $\mathcal{AHP}(T_n, T_j) = \mathbf{v}_n^{(j)}$, which could be easily converted to a distance metric using standard affinity-distance method $dist(T_n, T_j) = \gamma^{(j)} \exp(-\mathcal{AHP}(T_n, T_j))$. The scaling constant $\gamma^{(j)}$ would be optimized together with $\hat{e}^{(j)}$, modifying Eqn. 7 to:

$$\hat{e}^{(j)}, \gamma^{(j)} = \arg \min_{\hat{e}^{(j)}, \gamma^{(j)}} \sum_{n=1}^{j-1} (\|\hat{e}^{(j)} - e^{(n)}\|_2 - \gamma^{(j)} \exp(-\mathcal{AHP}(T_n, T_j)))^2. \quad (9)$$

⁴See Appendix A.2 for a brief proof and computation details.

Given that $H(T_n, T_j)$ and $e^{(n)}$ are actually given by calculation, the above optimization problem is a benign bi-variate optimization problem. We could thus apply a gradient descent algorithm to effectively compute the H-embedding $\hat{e}^{(j)}$ for the j -th task. As such, the H-embeddings for all tasks during the continual learning can be calculated in an inductive way.

4.2.2 Embedding Guidance via Encoder and Decoder

Building on this, we introduce an embedding regularization module to incorporate the H-embedding guidance into the hypernet. Viewing the hypernet as comprising a shallow encoder followed by a network, the task embedding e is first mapped from the embedding space \mathcal{E} to a hidden feature h in the hidden space \mathcal{H} , and subsequently to the weight space \mathcal{W} during the forward pass. For task j , we have:

$$\Theta^{(j)} = f_{h'}(h^{(j)}) = f_{h'}(f_{Enc}(e^{(j)})) = f_h(e^{(j)}). \quad (10)$$

Here, f_{Enc} and $f_{h'}$ denote the encoder and the rest part of hypernet respectively. From an information transmission perspective, we presume that the hypernet should in its hidden space encode sufficient information to recover the H-embedding \hat{e} . Therefore, we additionally introduce a shallow trainable decoder to map the hidden feature h to an embedding \tilde{e} such that the discrepancy between \tilde{e} and the H-embedding \hat{e} should be minimized, *i.e.*, for task j

$$\tilde{e}^{(j)} = f_{Dec}(h^{(j)}) = f_{Dec}(f_{Enc}(e^{(j)})) \quad (11)$$

should be as close to $\hat{e}^{(j)}$ as possible, where f_{Dec} denotes the decoder. Summarize it up in a mathematical form, we

Task	Cifar10/100			ImageNet-R		
Method	AA (↑)	BWT (↑)	FWT (↑)	AA (↑)	BWT (↑)	FWT (↑)
Finetune	18.32 ± 0.70	-66.98 ± 0.45	1.19 ± 0.48	15.08 ± 0.62	-41.34 ± 0.45	19.74 ± 0.98
Finetune Head	15.64 ± 0.21	-69.49 ± 0.73	0.00 ± 0.87	15.08 ± 0.62	-41.34 ± 0.45	19.74 ± 0.98
Multi Task	72.29 ± 0.12	- (N/A)	- (N/A)	14.34 ± 0.16	- (N/A)	- (N/A)
LwF	32.77 ± 0.52	-57.44 ± 0.57	6.72 ± 0.53	17.30 ± 0.05	-23.36 ± 0.27	3.39 ± 0.11
EWC	36.15 ± 1.48	-53.39 ± 1.69	6.38 ± 0.44	15.77 ± 0.29	-12.20 ± 0.34	-9.47 ± 0.74
L2	39.84 ± 0.67	-50.27 ± 0.79	7.13 ± 0.42	15.95 ± 0.39	-47.82 ± 0.56	26.34 ± 0.62
PredKD + FeatKD	33.03 ± 0.76	-56.19 ± 1.23	5.89 ± 0.31	18.22 ± 0.70	-22.15 ± 0.75	3.39 ± 0.11
PackNet	71.78 ± 0.11	- (N/A)	-7.15 ± 0.39	34.63 ± 0.85	- (N/A)	1.99 ± 0.93
HyperNet	82.21 ± 0.23	-0.05 ± 0.05	3.80 ± 0.53	38.03 ± 1.21	-0.15 ± 0.04	4.88 ± 0.80
WSN	82.87 ± 0.20	- (N/A)	4.92 ± 0.46	37.99 ± 0.27	- (N/A)	5.67 ± 0.56
H-embed Hnet*	83.58 ± 0.06	-0.02 ± 0.03	5.26 ± 0.45	38.16 ± 1.13	0.07 ± 0.09	4.80 ± 0.78

Table 1: **Accuracy (%) Comparison on Cifar10/100 and ImageNet-R.** All range of results are derived by three times running with different random seeds and calculating the average and standard deviation. Our method (marked by ‘*’) achieves the top average accuracy with high confidence.

have the embedding guidance loss for task j :

$$L_e = L_e(e^{(j)}, \hat{e}^{(j)}) = \mathcal{L}(f_{Dec}(f_{Enc}(e^{(j)})), \hat{e}^{(j)}). \quad (12)$$

\mathcal{L} denotes a certain similarity loss, set to the cosine similarity loss in our experiments. The H-embedding $\hat{e}^{(j)}$ is derived by Eqn. 10 and the decoder f_{Dec} is updated together with the hypernet during training. Notably, no significant computing cost is posed with the introduction of the embedding regularization module given the encoder and decoder are both shallow fully connected neural networks. We summarize the training process of task j as the algorithm in Appendix A.3.

5 EXPERIMENTS

5.1 EXPERIMENTAL SETTINGS

5.1.1 Benchmarks

To comprehensively verify the effectiveness of our framework and further analyze its reliability, we select three representative benchmarks from previous work on CL and perform extensive experiments on them: **PermutedMNIST** (10 tasks) [Goodfellow et al., 2013], **Cifar10/100** (11 tasks) [Krizhevsky et al., 2009], and **ImageNet-R** (10 tasks) [Hendrycks et al., 2021]⁵. A detailed description of these benchmarks is listed in Appendix A.4.

⁵Training specifics and detailed results of our experimental studies are listed in Appendix A.5, with codes available at https://anonymous.4open.science/r/H-embedding_guided_hypernet/.

5.1.2 Evaluation Metrics

Following our desiderata stated in Sec. 1 and previous works [Qu et al., 2021, Wang et al., 2024], we evaluate the different CL methods from three aspects:

- **Overall performance**, measured by average accuracy (AA) of the final model on all CL tasks:

$$AA = \frac{1}{M} \sum_{j=1}^M a_{j,M};$$

- **Memory degradation of old tasks**, measured by average backward transfer (BWT):

$$BWT = \frac{1}{M-1} \sum_{j=1}^{M-1} (a_{j,M} - a_{j,j});$$

- **Learning enhancement of new tasks**, measured by average forward transfer (FWT):

$$FWT = \frac{1}{M-1} \sum_{j=2}^M (a_{j,j} - \tilde{a}_j).$$

Here, $a_{i,j}$ denotes the accuracy (%) measured on the test set of i -th task after learning the j -th task, and \tilde{a}_j denotes the test accuracy derived by training a randomly initialized model directly on the j -th task. To conclude, a most desirable CL strategy should come with higher results on all three metrics, i.e. AA , BWT , and FWT .

5.2 PERFORMANCE EVALUATION

5.2.1 Comparison Experiments

Our primary evaluation study is conducted on the Cifar10/100 and ImageNet-R benchmarks with a total of 11

Setting	PermutedMNIST			Cifar10/100			ImageNet-R		
	MLP			CNN			ResNet-32		
Method	AA	BWT	FWT	AA	BWT	FWT	AA	BWT	FWT
Vanilla Hnet	97.495	0.007	0.063	69.679	-7.790	7.970	38.202	-0.105	6.817
Rand-embed Hnet	97.448	0.001	0.021	71.179	-6.140	7.970	38.046	0.090	6.448
H-embed Hnet*	97.553	-0.007	0.133	72.290	-5.328	8.380	39.212	-0.087	7.863

Table 2: **Ablation Study on different benchmarks and backbones.** Our H-embedding guidance proves to be effective across all three settings, attaining the highest average accuracy, with competitive backward transfer and the best forward transfer performance.

and 10 tasks respectively. To ensure fairness in comparison, a non-pre-trained ResNet-32 [He et al., 2016] is selected as the backbone model for all the chosen baselines. We reproduce all the methods with our own codes and each method is run three times with shared random seeds.

The choice of baselines is based on the requirements that they should both conform to our rehearsal-free setting and be applicable to the benchmark and backbone. For a thorough comparison with existing methods to the greatest extent possible, we select representative baselines of varied methodology categories, including: **Basic Methods:** Finetune, Finetune Head, Multi Task; **Regularization Methods:** LwF [Li and Hoiem, 2017], EWC [Kirkpatrick et al., 2017], L2, PredKD+FeatKD [Smith et al., 2023]; **Architecture Methods:** PackNet [Mallya and Lazebnik, 2018], HyperNet [von Oswald et al., 2020], WSN [Kang et al., 2022]. We summarize the experimental results in Table. 1. As can be seen from the table, our method performs prominently in the ultimate acquisition of CL tasks, achieving the highest final average accuracy. It also derives the best overall ability, displaying competitive performance in both forward and backward transfer.

5.2.2 Ablation Studies

To broaden the comprehensiveness of evaluation and take a better concentration on validating our introduction of H-embedding guidance, we conduct extra ablation studies on three differed settings with different benchmarks as well as model backbones. Namely, experimental settings include: PermutedMNIST (10 tasks) using an MLP model, Cifar10/100 (11 tasks) using a 4-layer CNN model, and ImageNet-R (10 tasks) using a ResNet-32 model. We compared across three methods where all hyperparameters are set exactly to the same: 1) Vanilla Hnet, the hypernet CL framework without guidance module; 2) Rand-embed Hnet, the same framework as ours but replacing H-embedding with a random embedding; 3) H-embed Hnet, our framework. The performance is evaluated and summarized in Table. 2, where a broad increase in CL performance could

be observed across all benchmarks and backbones.

5.3 DISCUSSION AND IN-DEPTH PERFORMANCE ANALYSIS

For a better analysis of the effectiveness of our strategy, we further investigate the detailed training behavior displayed in CL strategies, showing that our H-embedding guided hypernet is characterized by following superiority.

Optimal Overall Transfer Ability We select some of the best-performing baselines and plot their task-specific performance in Fig. 4. Each task is presented with two test accuracies: the accuracy obtained upon finishing training on the task, and the accuracy achieved by the final model after learning all CL tasks. As illustrated in the figures, our H-embedding guided hypernet demonstrates a notable advantage over Vanilla Hnet and WSN, exhibiting both effectiveness and stability in forward transfer while performing comparably in backward transfer. On the other hand, L2 as a regularization baseline, achieves good forward transfer ability, but fails in the mitigation of catastrophic forgetting. On the whole, our method displays a steady boost in forward transfer while retaining a competitive backward transfer, showcasing the best overall transfer ability, thereby attaining the highest average performance.

Quicker Convergence With the intention of understanding how our guidance aids the training process, we visualize the test accuracy trends during the training stage of tasks 1, 4, 7, 11 of the 11 CL tasks under Cifar-ResNet setting in Fig. 5. It is shown in the figures that, compared to a hypernet without H-embedding guidance, our method converges noticeably faster and achieves a higher final accuracy performance, especially with the growth of task numbers. Such a phenomenon serves as a further suggestion that our H-embedding guidance provides a substantial enhancement to the task learning in CL through forward transfer.

Embedding Interpretability To assess the task embeddings $\{e^{(j)}\}_{j=1}^M$ learned in our framework, we compute the

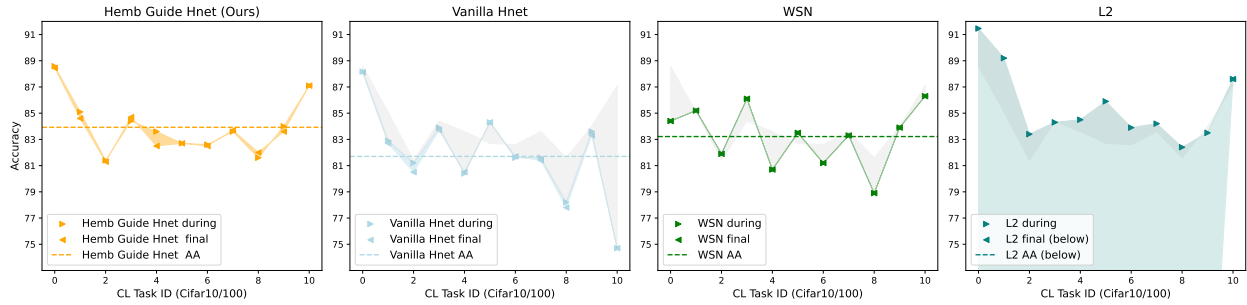


Figure 4: **The during and final task test accuracy of Cifar10/100 (ResNet-32 backbone, 100 epochs)**, with axis x for CL task IDs and axis y for the test accuracy. In the figures, \triangleright and \triangleleft denote the during and final accuracy, while the dashed line shows the average final accuracy and the colored region represents their discrepancy, *i.e.*, AA and BWT. From left to right is the accuracy visualization for H-embedding guided hypernet (ours), vanilla hypernet, WSN and L2 respectively. The grey regions in the right three figures denote the margin of during accuracy between these baselines and our method, *i.e.*, the discrepancy of FWT.

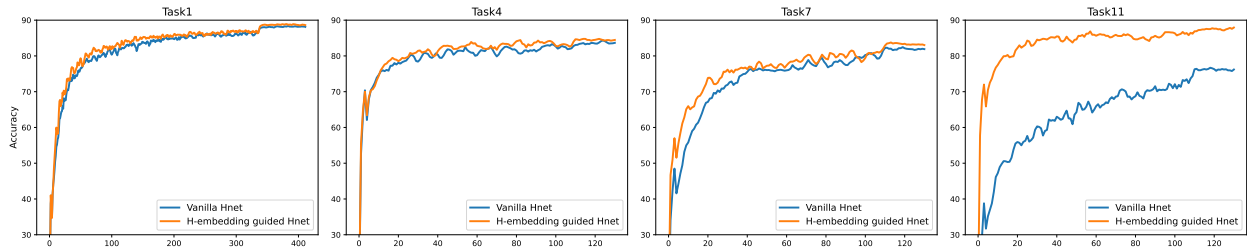


Figure 5: **Plotting of test accuracy during training task 1, 4, 7, 11 of Cifar10/100**, with axis x and y for the number of checkpoints and accuracy respectively. The blue curve represents the vanilla hypernet and the orange represents our H-embedding guided hypernet. As CL progresses, our method exhibits quicker convergence to higher accuracy in later tasks.

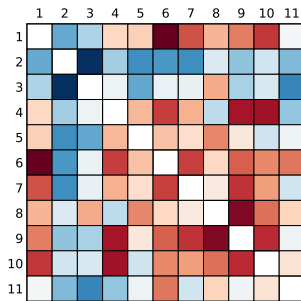


Figure 6: **Visualization of discrepancy between the task embedding distances learned w/ and w/o H-embedding guidance**. The grid of i -th row and j -th column represents the distance of task i and j . Darker cells indicate a larger discrepancy, with red for $d(w/) < d(w/o)$ and blue vice versa.

task-wise Euclidean distances of the embeddings obtained with and without H-embedding guidance, and visualize the discrepancy between these two distance matrix in Fig. 6. Red signifies that the with-guidance embeddings result in a closer distance between the two tasks compared to the without-guidance embeddings, while blue represents the opposite. Take task 9, a Cifar100 split task covering classes of

people and reptiles, as an instance. The embedding derived in our H-embedding guided hypernet successfully marks tasks 4, 6, 7, 8, 10 as more related, which all contain coverage of terrestrial animal classes or human scenarios. Our embedding also generally displays a greater preference for task 1, the more comprehensive Cifar10 task. Such correspondence with human intuition suggests a better capture of task interrelationships, leading to higher CL efficiency.

6 CONCLUSION

In this work, we propose a transferability-aware task embedding guided hypernet to exploit the task relationships for continual learning. By introducing the information theoretical transferability based task embedding named H-embedding and incorporating it in a hypernetwork, we establish an online framework capable of capturing the statistical relations among the CL tasks and leveraging this knowledge for guiding task-conditioned model weight generation. Through extensive experimental studies, we validate that the adoption of H-embedding guidance enhances continual learning by facilitating inter-task transfer and improving the reliability of task embeddings, achieving the best final accuracy performance under various CL benchmarks.

REFERENCES

- Andrea Agostinelli, Jasper Uijlings, Thomas Mensink, and Vittorio Ferrari. Transferability metrics for selecting source model ensembles. In *Proceedings of the IEEE/CVF Conference on Computer Vision and Pattern Recognition*, pages 7936–7946, 2022.
- Jihwan Bang, Heesu Kim, YoungJoon Yoo, Jung-Woo Ha, and Jonghyun Choi. Rainbow memory: Continual learning with a memory of diverse samples. In *Proceedings of the IEEE/CVF conference on computer vision and pattern recognition*, pages 8218–8227, 2021.
- Yajie Bao, Yang Li, Shao-Lun Huang, Lin Zhang, Lizhong Zheng, Amir Zamir, and Leonidas Guibas. An information-theoretic approach to transferability in task transfer learning. In *2019 IEEE international conference on image processing (ICIP)*, pages 2309–2313. IEEE, 2019.
- Eden Belouadah and Adrian Popescu. H2m: Class incremental learning with dual memory. In *Proceedings of the IEEE/CVF international conference on computer vision*, pages 583–592, 2019.
- Rich Caruana. Multitask learning. *Machine learning*, 28: 41–75, 1997.
- Vinod Kumar Chauhan, Jiandong Zhou, Ping Lu, Soheila Molaei, and David A Clifton. A brief review of hypernetworks in deep learning. *arXiv preprint arXiv:2306.06955*, 2023.
- Vinod Kumar Chauhan, Jiandong Zhou, Ghadeer Ghosheh, Soheila Molaei, and David A Clifton. Dynamic inter-treatment information sharing for individualized treatment effects estimation. In *International Conference on Artificial Intelligence and Statistics*, pages 3529–3537. PMLR, 2024.
- Jia Deng, Wei Dong, Richard Socher, Li-Jia Li, Kai Li, and Li Fei-Fei. Imagenet: A large-scale hierarchical image database. In *2009 IEEE conference on computer vision and pattern recognition*, pages 248–255. Ieee, 2009.
- Yuhe Ding, Bo Jiang, Aijing Yu, Aihua Zheng, and Jian Liang. Which model to transfer? a survey on transferability estimation. *arXiv preprint arXiv:2402.15231*, 2024.
- Hans Gebelein. Das statistische problem der korrelation als variations-und eigenwertproblem und sein zusammenhang mit der ausgleichsrechnung. *ZAMM-Journal of Applied Mathematics and Mechanics/Zeitschrift für Angewandte Mathematik und Mechanik*, 21(6):364–379, 1941.
- Ian J Goodfellow, Mehdi Mirza, Da Xiao, Aaron Courville, and Yoshua Bengio. An empirical investigation of catastrophic forgetting in gradient-based neural networks. *arXiv preprint arXiv:1312.6211*, 2013.
- David Ha, Andrew M Dai, and Quoc V Le. Hypernetworks. In *International Conference on Learning Representations*, 2017.
- Kaiming He, Xiangyu Zhang, Shaoqing Ren, and Jian Sun. Deep residual learning for image recognition. In *Proceedings of the IEEE conference on computer vision and pattern recognition*, pages 770–778, 2016.
- Dan Hendrycks, Steven Basart, Norman Mu, Saurav Kadavath, Frank Wang, Evan Dorundo, Rahul Desai, Tyler Zhu, Samyak Parajuli, Mike Guo, et al. The many faces of robustness: A critical analysis of out-of-distribution generalization. In *Proceedings of the IEEE/CVF international conference on computer vision*, pages 8340–8349, 2021.
- Hermann O Hirschfeld. A connection between correlation and contingency. In *Mathematical Proceedings of the Cambridge Philosophical Society*, volume 31, pages 520–524. Cambridge University Press, 1935.
- YenChang Hsu, YenCheng Liu, Anita Ramasamy, and Zsolt Kira. Re-evaluating continual learning scenarios: A categorization and case for strong baselines. continual learning workshop. In *32nd Conference on Neural Information Processing Systems*, 2018.
- Shao-Lun Huang, Xiangxiang Xu, Lizhong Zheng, and Gregory W Wornell. An information theoretic interpretation to deep neural networks. In *2019 IEEE International Symposium on Information Theory (ISIT)*, pages 1984–1988. IEEE, 2019.
- Shibal Ibrahim, Natalia Ponomareva, and Rahul Mazumder. Newer is not always better: Rethinking transferability metrics, their peculiarities, stability and performance. In *Joint European Conference on Machine Learning and Knowledge Discovery in Databases*, pages 693–709. Springer, 2022.
- Hyundong Jin and Eunwoo Kim. Helpful or harmful: Intertask association in continual learning. In *European Conference on Computer Vision*, pages 519–535. Springer, 2022.
- Haeyong Kang, Rusty John Lloyd Mina, Sultan Rizky Hikmawan Madjid, Jaehong Yoon, Mark Hasegawa-Johnson, Sung Ju Hwang, and Chang D Yoo. Forget-free continual learning with winning subnetworks. In *International Conference on Machine Learning*, pages 10734–10750. PMLR, 2022.
- James Kirkpatrick, Razvan Pascanu, Neil Rabinowitz, Joel Veness, Guillaume Desjardins, Andrei A Rusu, Kieran Milan, John Quan, Tiago Ramalho, Agnieszka Grabska-Barwinska, et al. Overcoming catastrophic forgetting in neural networks. *Proceedings of the national academy of sciences*, 114(13):3521–3526, 2017.

- Alex Krizhevsky, Geoffrey Hinton, et al. Learning multiple layers of features from tiny images. 2009.
- David Krueger, Chin-Wei Huang, Riashat Islam, Ryan Turner, Alexandre Lacoste, and Aaron Courville. Bayesian hypernetworks. *arXiv preprint arXiv:1710.04759*, 2017.
- Yann LeCun, Léon Bottou, Yoshua Bengio, and Patrick Haffner. Gradient-based learning applied to document recognition. *Proceedings of the IEEE*, 86(11):2278–2324, 1998.
- Zhizhong Li and Derek Hoiem. Learning without forgetting. *IEEE transactions on pattern analysis and machine intelligence*, 40(12):2935–2947, 2017.
- Arun Mallya and Svetlana Lazebnik. Packnet: Adding multiple tasks to a single network by iterative pruning. In *Proceedings of the IEEE conference on Computer Vision and Pattern Recognition*, pages 7765–7773, 2018.
- Cuong Nguyen, Tal Hassner, Matthias Seeger, and Cedric Archambeau. Leep: A new measure to evaluate transferability of learned representations. In *International Conference on Machine Learning*, pages 7294–7305. PMLR, 2020.
- Haoxuan Qu, Hossein Rahmani, Li Xu, Bryan Williams, and Jun Liu. Recent advances of continual learning in computer vision: An overview. *arXiv preprint arXiv:2109.11369*, 2021.
- Sylvestre-Alvise Rebuffi, Alexander Kolesnikov, Georg Sperl, and Christoph H Lampert. icarl: Incremental classifier and representation learning. In *Proceedings of the IEEE conference on Computer Vision and Pattern Recognition*, pages 2001–2010, 2017.
- Alfréd Rényi. On measures of dependence. *Acta mathematica hungarica*, 10(3-4):441–451, 1959.
- Elad Sarafian, Shai Keynan, and Sarit Kraus. Recomposing the reinforcement learning building blocks with hypernetworks. In *International Conference on Machine Learning*, pages 9301–9312. PMLR, 2021.
- Marcin Sendera, Marcin Przewięźlikowski, Konrad Karanowski, Maciej Zięba, Jacek Tabor, and Przemysław Spurek. Hypershot: Few-shot learning by kernel hypernetworks. In *Proceedings of the IEEE/CVF winter conference on applications of computer vision*, pages 2469–2478, 2023.
- Hanul Shin, Jung Kwon Lee, Jaehong Kim, and Jiwon Kim. Continual learning with deep generative replay. *Advances in neural information processing systems*, 30, 2017.
- James Seale Smith, Junjiao Tian, Shaunak Halbe, Yen-Chang Hsu, and Zsolt Kira. A closer look at rehearsal-free continual learning. In *Proceedings of the IEEE/CVF conference on computer vision and pattern recognition*, pages 2410–2420, 2023.
- Yang Tan, Yang Li, and Shao-Lun Huang. Otce: A transferability metric for cross-domain cross-task representations. In *Proceedings of the IEEE/CVF conference on computer vision and pattern recognition*, pages 15779–15788, 2021.
- Yang Tan, Enming Zhang, Yang Li, Shao-Lun Huang, and Xiao-Ping Zhang. Transferability-guided cross-domain cross-task transfer learning. *IEEE Transactions on Neural Networks and Learning Systems*, 2024.
- Anh T Tran, Cuong V Nguyen, and Tal Hassner. Transferability and hardness of supervised classification tasks. In *Proceedings of the IEEE/CVF International Conference on Computer Vision*, pages 1395–1405, 2019.
- Gido M Van de Ven and Andreas S Tolias. Three scenarios for continual learning. *arXiv preprint arXiv:1904.07734*, 2019.
- Tomer Volk, Eyal Ben-David, Ohad Amosy, Gal Chechik, and Roi Reichart. Example-based hypernetworks for out-of-distribution generalization. *arXiv preprint arXiv:2203.14276*, 2022.
- Johannes von Oswald, Christian Henning, Benjamin F Grewe, and João Sacramento. Continual learning with hypernetworks. In *8th International Conference on Learning Representations (ICLR 2020)(virtual)*. International Conference on Learning Representations, 2020.
- L Wang, X Zhang, H Su, and J Zhu. A comprehensive survey of continual learning: Theory, method and application. *IEEE Transactions on Pattern Analysis and Machine Intelligence*, 2024.
- Mitchell Wortsman, Vivek Ramanujan, Rosanne Liu, Aniruddha Kembhavi, Mohammad Rastegari, Jason Yosinski, and Ali Farhadi. Supermasks in superposition. *Advances in Neural Information Processing Systems*, 33: 15173–15184, 2020.
- Yanru Wu, Jianning Wang, Weida Wang, and Yang Li. H-ensemble: An information theoretic approach to reliable few-shot multi-source-free transfer. In *Proceedings of the AAAI Conference on Artificial Intelligence*, volume 38, pages 15970–15978, 2024.
- Kaichao You, Yong Liu, Jianmin Wang, and Mingsheng Long. Logme: Practical assessment of pre-trained models for transfer learning. In *International Conference on Machine Learning*, pages 12133–12143. PMLR, 2021.

Amir R Zamir, Alexander Sax, William Shen, Leonidas J Guibas, Jitendra Malik, and Silvio Savarese. Taskonomy: Disentangling task transfer learning. In *Proceedings of the IEEE conference on computer vision and pattern recognition*, pages 3712–3722, 2018.

Friedemann Zenke, Ben Poole, and Surya Ganguli. Continual learning through synaptic intelligence. In *International conference on machine learning*, pages 3987–3995. PMLR, 2017.

Supplementary Material

Yanru Wu¹ Xiangyu Chen¹ Jianning Wang² Enming Zhang¹ Hanbing Liu¹ Yang Li^{1†}

* Corresponding author

¹Shenzhen Key Laboratory of Ubiquitous Data Enabling, Shenzhen International Graduate School, Tsinghua University

²Independent Researcher

A APPENDIX

A.1 CONTINUAL LEARNING SETTING

Based on the discrepancy between D_{j-1} and D_j , Hsu et al. [2018] and Van de Ven and Tolias [2019] categorize CL settings into three specific scenarios: task incremental, class incremental, and domain incremental. Table 3 summarizes the differences among these scenarios. For a better concentration on the study of CL methodology, our work mainly focuses on the task incremental CL. In this scenario, the output spaces of tasks are partitioned by task IDs and mutually exclusive between D_{j-1} and D_j , which is denoted as $\mathbf{Y}^{(j-1)} \neq \mathbf{Y}^{(j)}$. It can be then naturally indicated that $P(\mathbf{Y}^{(j-1)}) \neq P(\mathbf{Y}^{(j)})$ and $P(\mathbf{X}^{(j-1)}) \neq P(\mathbf{X}^{(j)})$. Notably, here task IDs are accessible during both training and testing. An adaptation of our method to other CL settings could be effectively conducted by introducing additional task inference modules similar to previous works.

Scenario	$P(\mathbf{X}^{(j-1)}) \neq P(\mathbf{X}^{(j)})$	$P(\mathbf{Y}^{(j-1)}) \neq P(\mathbf{Y}^{(j)})$	$\mathbf{Y}^{(j-1)} \neq \mathbf{Y}^{(j)}$	Task ID
Domain Incremental	✓	✗	✗	✗
Class Incremental	✓	✓	✗	✗
Task Incremental*	✓	✓	✓	✓

Table 3: **Categorization of CL settings based on the discrepancy between D_{j-1} and D_j .** ‘*’ denotes the scenario focused on in our work.

A.2 HGR MAXIMAL CORRELATION FOR SELF TRANSFERABILITY $H(T_j, T_j)$

As the theoretical basis of H-score transferability, the Hirschfeld–Gebelein–Rényi (HGR) maximal correlation of random variables X and Y over alphabets \mathcal{X} and \mathcal{Y} is defined as:

$$\begin{aligned}
 \mathcal{HGR}(X, Y) = & \max_{\substack{f: \mathcal{X} \rightarrow \mathbb{R}^k, g: \mathcal{Y} \rightarrow \mathbb{R}^k \\ \mathbb{E}[f(X)] = \mathbb{E}[g(Y)] = \mathbf{0} \\ \mathbb{E}[f(X)f^\top(X)] = \mathbb{E}[g(Y)g^\top(Y)] = \mathbf{I}}} \mathbb{E}_{P_{XY}} [f^\top(X)g(Y)]. \quad (13)
 \end{aligned}$$

Here, the correlation is derived by taking the maximum over all functions f, g with zero mean and unit variance, which hence extracts the most correlated aspects of X and Y . This definition is equivalent to the maximum of the two-sided H-score given by Huang et al. [2019] with normalized functions f and g :

$$H(f, g) = \mathbb{E}_{P_{XY}} [f^\top(X)g(Y)] - \frac{1}{2} \text{tr}(\text{cov}(f(X))\text{cov}(g(Y))), \quad (14)$$

with the one-sided H-score extended from Eqn. 14 by assuming the function g as optimal:

$$H(f) = \text{tr}(\text{cov}(f(X))^{-1} \text{cov}(\mathbb{E}_{P_{X|Y}}[f(X)|Y])). \quad (15)$$

Notably, Eqn. 15 is exactly the definition of H-score transferability [Bao et al., 2019], which is actually proposed by applying the H-score theories to transfer learning scenarios. Therefore, with normalized f, g , the HGR maximal correlation between X_j, Y_j is mathematically equivalent to the H-score metric of the theoretical optimal model f_j^* on task j .

In our work, we utilize the H-score transferability metrics denoted as $H(T_i, T_j)$ for tasks $i \neq j$. However, the H-score for task j cannot be computed while the model remains untrained for that specific task. To maintain consistency in our definitions, we define $H(T_j, T_j)$ as the HGR maximal correlation between the input X_j and the output Y_j , implicitly leveraging the theoretical optimal model f_j^* for task j . Specifically, in our computations, the models f and g are implemented as fully connected neural networks equipped with normalization layers, and they undergo 100 epochs of training using a sampled subset of the training data through gradient descent.

A.3 ALGORITHM FOR H-EMBEDDING GUIDED HYPERNET FRAMEWORK

For a better understanding of our framework, we summarize the entire training process of task j within our H-embedding guided hypernet as outlined in Algorithm. 1

Algorithm 1: H-embedding guided Hypernet: Training of Task j

Input: Task data D_j , previous task embeddings $\{e^{(n)}\}_{n=1}^{j-1}$, hypernet weights Θ_h

Parameter : Learning rate λ

Output: Current task embedding $e^{(j)}$, updated hypernet weights Θ_h

Randomly initialize $e^{(j)}, \hat{e}^{(j)}$;

if $j > 2$ **then**

for $n \leftarrow 1$ **to** $j - 1$ **do** // Compute transferability

$\Theta^{(n)} \leftarrow f_h(e^{(n)}, \Theta_h)$;

$H(T_n, T_j) \leftarrow \text{tr}(\text{cov}(f_l(x^{(j)}, \Theta^{(n)}))^{-1} \text{cov}(\mathbb{E}_{P_{X|Y}}[f_l(x^{(j)}, \Theta^{(n)})|y^{(j)}]))$ ▷ Eq. 6

end

 Randomly initialize $\gamma^{(j)}$;

$\hat{e}^{(j)}, \gamma^{(j)} \leftarrow \arg \min_{\hat{e}^{(j)}, \gamma^{(j)}} \sum_{n=1}^{j-1} (\|\hat{e}^{(j)} - e^{(n)}\|_2 - \gamma^{(j)} \exp(-\mathcal{AHP}(T_n, T_j)))^2$ ▷ Eq. 10

end

repeat // Train hypernet

$e^{(j)} \leftarrow e^{(j)} - \lambda \nabla_{e^{(j)}} L$;

$\Theta_h \leftarrow \Theta_h - \lambda \nabla_{\Theta_h} L$ ▷ Eq. 5

until *converge*;

Return $e^{(j)}, f_h(\cdot, \Theta_h)$

A.4 BENCHMARKS OF EXPERIMENTS

PermutedMNIST [Goodfellow et al., 2013] benchmark is a variant of MNIST [LeCun et al., 1998], forming CL tasks from the original MNIST dataset by applying random permutations to the input image pixels. The permuting procedure can be repeated in experiments to yield a task sequence of desired length, with each task consisting of 70,000 images (60,000 for training and 10,000 for testing) of digits from 0 to 9. **Cifar10/100** is a benchmark composed of 11 ten-way classification tasks, with a full Cifar10 task and a Cifar100 dataset split into ten tasks [Krizhevsky et al., 2009]. The model is firstly trained on the Cifar10 task with 60,000 images (50,000 for training and 10,000 for testing) and then sequentially trained on the ten Cifar100 tasks, each with 6,000 images (5,000 for training and 1,000 for testing). **ImageNet-R** [Hendrycks et al., 2021], built upon the ImageNet dataset [Deng et al., 2009], features a diverse range of renditions of ImageNet classes. This benchmark includes a total of 30,000 images across 200 classes from ImageNet. For continual learning evaluation, ImageNet-R is organized into 10 tasks, each containing 20 classes and around 3,000 samples (roughly 2,500 for training and 500 for testing).

A.5 EXPERIMENTAL SETTINGS

A.5.1 Comparison Experiments

Choice of Baselines. Our selection of baselines in this work aims to encompass a wide range of baseline categories, covering two of three primary categories in contemporary CL researches (*i.e.*, replay-based, regularization-based, and architecture-based), with the replay-based methods not conforming to our rehearsal-free setting. The specific choice of baselines in each category is mainly based on performance comparison conclusions in recent works such as Smith et al. [2023] and Kang et al. [2022]. Therefore, we believe that our comparison study has included the most competitive and representative baselines.

General Settings. In CIFAR10/100 and ImageNet-R datasets using a ResNet-32 backbone network without pre-training, we evaluate several baseline methods including Finetune, Finetune-Head, EWC, L2, PredKD+FeatKD, PackNet, HyperNet, WSN. The ResNet-32 uses ‘option A’, *i.e.*, leveraging the zero-padding shortcuts for increasing dimensions, as indicated in CIFAR-10 experiments of the original ResNet paper Sec4.2. The experiments on CIFAR10/100 are conducted on NVIDIA GeForce RTX 3090 GPUs with 100 epochs of training (unless early-stop), and the ImageNet-R experiments are carried out on NVIDIA A800 or A100 GPUs with 200 epochs of training (unless early-stop).

To ensure a fair comparison, we adopt consistent training settings across all baseline methods (unless listed separately). Specifically, the batch size is set to 32, and each task is trained for 100 epochs. We use the Adam optimizer with an initial learning rate of 0.001. The learning rate is decayed by a factor of 10 after the 50th and 75th epochs. A weight decay of 1×10^{-4} is applied. For robustness, each experiment is run three times with different random seeds 22, 32, and 42, and the results are averaged.

Details of Specific Methods. For the **Finetune** baseline, the model is sequentially trained on each task without any mechanisms to prevent catastrophic forgetting. The model is randomly initialized and trained from scratch on the first task. The training of subsequent tasks continues using the weights obtained from the previous task.

In the **Finetune-Head** baseline, all convolutional layers of the ResNet-32 model are frozen after training on the first task. When learning new tasks, only the parameters of the final fully connected layer (the classifier) are updated. This approach aims to retain the feature representations learned from earlier tasks while adapting the classifier to new task-specific outputs.

In the **Multi Task** baseline, the dataset is trained as a whole (instead of split into 10/11 tasks) using a non-pretrained ResNet-32 until convergence. We then separately test the classification accuracy on each split and take an average to get the AA metric.

For the **EWC** baseline [Kirkpatrick et al., 2017], we add a regularization term to the loss function to penalize significant changes to parameters important for previously learned tasks. The importance of each parameter is estimated using the Fisher Information Matrix. The regularization coefficient λ is set to 10, following standard practice.

In the **L2** baseline, an L2 regularization term is added to the loss function to limit changes in the model parameters during training on new tasks. The regularization coefficient λ is set to 1.0, determined by tuning on a small validation set derived from the training data of the first task.

For the **PredKD + FeatKD** method [Smith et al., 2023], we incorporate both prediction distillation and feature distillation to transfer knowledge from previous tasks to new ones. The distillation loss combines the Kullback-Leibler divergence between the soft outputs of the teacher (model trained on previous tasks) and the student (current model), as well as the mean squared error between their intermediate feature representations. The loss weights are set to $\alpha = 1.0$ and $\beta = 0.5$ based on preliminary tuning.

In the **PackNet** method [Mallya and Lazebnik, 2018], we employ iterative pruning to allocate dedicated network weights for each task. After training on each task, we prune a certain percentage of the weights with the smallest magnitudes. Following the recommendations in the original paper, we experiment with pruning rates of 0.5, 0.75, and 0.8. We select the pruning rate of 0.8, which yields the best performance in our setting. After pruning, we fine-tune the remaining weights for an additional 10 epochs with a reduced learning rate of 1×10^{-4} .

For **HyperNet** method [von Oswald et al., 2020], we primarily follow the original work in training settings, with the learning rate being 0.001, the CL loss beta being 0.05, and scheduling and transforming strategies being the same as those used by Oswald. The embedding dimension is set to 32.

For the **WSN** method [Kang et al., 2022], we follow its original paper and use the default values of parameters in its official code repository. We choose the sparsity parameter $c = 0.5$ which perform best as listed in the WSN literature. Other parameters are set to the following values: optimization via Adam, a learning rate initialize at $1e-3$ with a minimum of $1e-6$, and a patience of 6 epochs for reducing the learning rate by a factor of 2. The models are trained for 100 epochs, with a batch size of 64 for both training and testing.

For our **H-embedding guided hypernet**, the learning rate is set to 0.0005, with the embedding loss beta and CL loss beta both set to 0.05. The scheduling and transforming strategies are set the same as those of von Oswald et al. [2020] and the embedding dimension is also set to 32. For the learning of H-embedding, we update Eqn. 10 using gradient descent for 2000 iterations and the f, g in HGR maximal correlation for 100 epochs respectively, both using a subset of 1000 samples from the training set.

In all methods, we adhere to the principles of continual learning by not tuning hyperparameters on the full task set. Special care was taken in handling batch normalization layers, especially in methods involving parameter freezing or pruning. Following the settings in von Oswald et al. [2020], we store and update batch normalization statistics separately for each task to ensure proper normalization during both training and inference.

A.5.2 Ablation Studies

ImageNet-R For the ImageNet-R dataset, we split the original 200 classes into ten 20-way classification tasks. Because of the uneven class sample size of ImageNet dataset, each task has varied numbers of training and test samples: Task 1 with 2,166 training samples and 543 test samples, Task 2 with 2,655 training and 716 test samples, . . . , until Task 9 with 2,058 training samples and 471 test samples. In our method, we use a learning rate of 0.0005 and a the embedding loss beta of 0.05, training the models for 200 epochs. The backbone model is the same as used in comparison experiments. The results are derived on NVIDIA A100 GPUs.

Cifar10/100 The tasks in this setting are derived the same as in comparison studies. Yet, the backbone model is differently set to a 4-layer CNN as used by Zenke et al. [2017]. We also follow Oswald in most of the hyperparameters, configuring learning rate to 0.0001, embedding size to 32, as well as using the same scheduling strategies. We train each method with 100 epochs and the embedding loss beta is set to 0.2 for H-embed and rand-embed hypernets. The results are derived on NVIDIA GeForce RTX 3090 GPUs.

PermutedMNIST Considering the smaller data dimension and model size in this setting, the embedding size is reduced to 24 and training iteration number is set to 5000. The backbone model on PermutedMNIST is selected to be an MLP with fully-connected layers of size 1000, 1000 as used by Van de Ven and Tolias [2019]. We configure the learning rate as 0.0001 and the embedding loss beta as 0.05. The results are derived on NVIDIA GeForce RTX 3090 GPUs.

A.6 DETAILED EXPERIMENTAL RESULTS

Considering the limited space, we only present the experimental results measured by our three metrics in main text. Here, we list the whole continual learning performance below. The during accuracy refers to the test accuracy of tasks upon finishing training on that task, and the final accuracy refers to the test accuracy of tasks when finishing learning all CL tasks. The results of comparison experiments are derived with three times running of seed 22, 32, 42 and the ablation studies are conducted a single time only.

Method	Task 1	Task 2	Task 3	Task 4	Task 5	Task 6	Task 7	Task 8	Task 9	Task 10	Task 11
Finetune	81.14 ± 0.32	79.10 ± 0.91	76.70 ± 0.85	79.97 ± 1.89	78.57 ± 2.40	79.97 ± 1.41	78.20 ± 1.92	79.70 ± 1.93	74.77 ± 1.46	80.43 ± 0.93	82.77 ± 2.08
Finetune Head	88.65 ± 1.11	77.90 ± 3.12	76.57 ± 1.99	76.03 ± 4.46	77.80 ± 2.38	78.13 ± 1.03	76.80 ± 1.51	79.33 ± 2.10	75.00 ± 1.04	81.20 ± 0.85	79.53 ± 0.65
LwF	89.39 ± 1.64	87.17 ± 0.45	84.37 ± 0.63	85.10 ± 0.99	83.83 ± 0.45	85.53 ± 0.85	82.07 ± 0.86	84.17 ± 0.45	82.37 ± 0.38	84.03 ± 1.70	86.83 ± 0.59
EWC	89.39 ± 1.64	86.57 ± 0.34	83.63 ± 1.14	86.10 ± 0.43	84.70 ± 1.36	85.67 ± 0.71	82.73 ± 1.23	82.30 ± 1.42	81.67 ± 0.91	83.13 ± 0.66	85.60 ± 1.92
L2	91.27 ± 0.27	87.33 ± 1.34	84.07 ± 0.81	85.97 ± 1.28	85.53 ± 1.07	85.00 ± 0.83	84.20 ± 0.24	84.57 ± 0.33	81.27 ± 0.80	84.30 ± 0.86	87.33 ± 0.21
PredKD+FeatKD	88.66 ± 0.85	86.50 ± 0.28	82.70 ± 0.71	86.03 ± 0.47	85.80 ± 0.99	86.07 ± 0.24	83.60 ± 0.00	81.17 ± 0.52	81.10 ± 0.99	83.63 ± 0.09	85.43 ± 1.79
Packnet	82.79 ± 0.20	73.07 ± 0.63	69.03 ± 0.39	76.20 ± 0.78	69.47 ± 1.35	71.40 ± 0.99	68.07 ± 1.69	71.43 ± 0.62	67.13 ± 0.47	66.47 ± 0.34	74.50 ± 0.54
WSN	84.03 ± 0.26	83.63 ± 1.13	80.50 ± 1.10	84.80 ± 0.93	81.30 ± 0.45	83.53 ± 0.21	80.27 ± 0.68	83.27 ± 0.29	78.77 ± 1.55	84.87 ± 0.82	86.57 ± 0.60
Vanilla Hnet	88.52 ± 0.37	82.87 ± 0.29	80.47 ± 0.52	83.30 ± 0.43	81.97 ± 1.17	83.30 ± 0.78	80.37 ± 1.34	80.60 ± 2.79	79.13 ± 0.93	82.00 ± 1.35	82.30 ± 5.45
H-embed Hnet*	88.78 ± 0.11	83.35 ± 0.15	82.10 ± 0.30	83.55 ± 0.05	81.10 ± 0.70	82.90 ± 1.40	83.05 ± 1.05	81.55 ± 1.05	81.10 ± 1.50	84.55 ± 0.15	87.15 ± 0.65

Table 4: **Cifar-Comparison Experiments, Accuracy During.** The test accuracy of tasks upon finishing training on that task. The mean value and standard deviation are derived with three times running.

Method	Task 1	Task 2	Task 3	Task 4	Task 5	Task 6	Task 7	Task 8	Task 9	Task 10	Task 11
Finetune	10.21 ± 0.30	10.27 ± 0.77	10.00 ± 0.00	9.63 ± 0.52	11.80 ± 1.81	11.83 ± 2.66	11.07 ± 2.66	10.90 ± 1.65	13.23 ± 3.44	19.77 ± 1.19	82.77 ± 2.08
Finetune Head	9.48 ± 0.76	7.97 ± 0.94	8.70 ± 0.28	8.13 ± 0.24	9.80 ± 0.28	6.57 ± 2.03	11.07 ± 0.66	9.80 ± 1.84	9.73 ± 0.24	8.60 ± 0.99	79.00 ± 0.42
LwF	16.93 ± 1.30	17.77 ± 2.29	19.77 ± 1.72	18.83 ± 0.82	21.97 ± 0.74	23.00 ± 1.59	26.27 ± 1.68	35.70 ± 4.15	40.30 ± 4.14	53.07 ± 0.50	86.83 ± 0.59
EWC	19.34 ± 4.27	18.00 ± 3.76	23.23 ± 3.93	25.10 ± 3.77	24.97 ± 2.77	30.00 ± 6.34	31.67 ± 3.60	40.87 ± 2.17	41.03 ± 7.99	57.80 ± 5.03	85.60 ± 1.92
L2	23.32 ± 5.53	21.60 ± 3.27	25.10 ± 0.86	25.17 ± 5.00	29.30 ± 2.79	27.83 ± 5.42	41.07 ± 3.13	49.30 ± 6.23	51.23 ± 2.01	56.93 ± 1.61	87.33 ± 0.21
PredKD+FeatKD	19.12 ± 5.04	15.53 ± 2.29	23.37 ± 1.69	20.80 ± 1.27	19.93 ± 2.15	25.23 ± 4.86	23.90 ± 0.41	32.93 ± 5.14	43.77 ± 3.30	51.73 ± 4.43	87.07 ± 0.17
Packnet	82.79 ± 0.20	73.07 ± 0.63	69.03 ± 0.39	76.20 ± 0.78	69.47 ± 1.35	71.40 ± 0.99	68.07 ± 1.69	71.43 ± 0.62	67.13 ± 0.47	66.47 ± 0.34	74.50 ± 0.54
WSN	84.03 ± 0.26	83.63 ± 1.13	80.50 ± 1.10	84.80 ± 0.93	81.30 ± 0.45	83.53 ± 0.21	80.27 ± 0.68	83.27 ± 0.29	78.77 ± 1.55	84.87 ± 0.82	86.57 ± 0.60
Vanilla Hnet	88.55 ± 0.37	82.73 ± 0.37	80.13 ± 0.33	83.40 ± 0.24	82.00 ± 1.07	83.27 ± 0.82	80.43 ± 1.58	80.53 ± 2.60	78.97 ± 1.08	81.97 ± 1.20	82.30 ± 5.45
H-embed Hnet*	88.71 ± 0.01	83.50 ± 0.00	82.05 ± 0.15	83.60 ± 0.40	81.05 ± 0.45	82.65 ± 1.65	83.00 ± 1.10	81.35 ± 1.15	81.10 ± 1.40	84.50 ± 0.30	87.15 ± 0.65

Table 5: **Cifar-Comparison Experiments, Accuracy Final.** The test accuracy of tasks when finishing learning all CL tasks. The mean value and standard deviation are derived with three times running.

Method	Task 1	Task 2	Task 3	Task 4	Task 5	Task 6	Task 7	Task 8	Task 9	Task 10
Finetune	46.84 ± 2.93	39.80 ± 3.18	51.84 ± 2.02	47.96 ± 3.32	59.19 ± 3.32	51.93 ± 1.85	56.61 ± 1.63	56.92 ± 1.74	53.83 ± 2.30	57.96 ± 0.69
Finetune Head	46.84 ± 2.93	39.80 ± 3.18	51.84 ± 2.02	47.96 ± 3.32	59.19 ± 3.32	51.93 ± 1.85	56.61 ± 1.63	56.92 ± 1.74	53.83 ± 2.30	57.96 ± 0.69
LwF	54.39 ± 0.76	37.80 ± 0.43	41.95 ± 1.99	33.24 ± 1.43	42.80 ± 0.88	32.86 ± 0.37	36.62 ± 0.51	32.44 ± 0.85	31.06 ± 0.49	40.06 ± 0.99
EWC	54.39 ± 0.76	33.38 ± 0.82	30.74 ± 2.07	20.02 ± 1.37	24.89 ± 2.86	18.54 ± 1.11	23.70 ± 1.83	18.76 ± 0.93	18.06 ± 2.32	25.05 ± 2.17
L2	54.39 ± 0.76	51.58 ± 0.76	58.59 ± 1.48	54.13 ± 1.19	65.54 ± 0.53	58.43 ± 2.28	63.55 ± 1.54	61.37 ± 0.66	58.49 ± 1.53	63.77 ± 0.70
PredKD+FeatKD	54.39 ± 0.76	37.80 ± 0.43	41.95 ± 1.99	33.24 ± 1.43	42.80 ± 0.88	32.86 ± 0.37	36.62 ± 0.51	32.44 ± 0.85	31.06 ± 0.49	40.06 ± 0.99
Packnet	30.08 ± 2.94	34.96 ± 3.33	38.34 ± 2.81	31.97 ± 0.96	46.02 ± 1.68	29.37 ± 1.37	35.67 ± 1.54	32.23 ± 1.18	33.56 ± 1.50	34.11 ± 1.74
WSN	30.53 ± 2.80	29.63 ± 1.11	33.97 ± 1.49	29.63 ± 2.45	46.77 ± 1.02	36.57 ± 1.11	43.60 ± 0.83	41.67 ± 0.90	41.60 ± 1.31	45.97 ± 2.00
Vanilla Hnet	39.41 ± 3.94	30.31 ± 1.10	40.02 ± 2.11	36.25 ± 1.81	44.41 ± 0.50	33.81 ± 1.94	41.47 ± 2.64	38.00 ± 2.50	34.13 ± 5.32	43.88 ± 2.08
H-embed Hnet*	39.41 ± 3.94	30.31 ± 1.10	39.78 ± 2.47	35.71 ± 1.68	43.92 ± 1.24	35.55 ± 2.09	39.62 ± 2.27	37.89 ± 1.22	34.07 ± 3.96	44.73 ± 2.05

Table 6: **ImageNet.Comparison Experiments, Accuracy During.** The test accuracy of tasks upon finishing training on that task. The mean value and standard deviation are derived with three times running.

Method	Task 1	Task 2	Task 3	Task 4	Task 5	Task 6	Task 7	Task 8	Task 9	Task 10
Finetune	7.67 ± 0.31	7.03 ± 2.83	9.04 ± 2.43	10.79 ± 1.49	9.46 ± 2.20	6.18 ± 0.81	15.32 ± 2.08	10.48 ± 0.71	16.87 ± 2.92	57.96 ± 0.69
Finetune Head	7.67 ± 0.31	7.03 ± 2.83	9.04 ± 2.43	10.79 ± 1.49	9.46 ± 2.20	6.18 ± 0.81	15.32 ± 2.08	10.48 ± 0.71	16.87 ± 2.92	57.96 ± 0.69
LwF	8.04 ± 1.66	11.96 ± 1.52	11.63 ± 1.18	9.57 ± 2.10	17.63 ± 2.40	16.90 ± 1.30	18.49 ± 2.11	17.77 ± 1.16	20.95 ± 1.10	40.06 ± 0.99
EWC	6.88 ± 1.43	11.92 ± 0.67	14.23 ± 0.90	11.42 ± 1.11	17.04 ± 1.54	15.37 ± 1.23	20.89 ± 1.18	16.93 ± 1.00	18.00 ± 1.62	25.05 ± 2.17
L2	10.37 ± 0.92	6.10 ± 1.14	8.26 ± 0.43	9.96 ± 0.30	10.75 ± 1.19	7.66 ± 1.20	16.10 ± 3.10	9.64 ± 0.63	16.87 ± 2.43	63.77 ± 0.70
PredKD+FeatKD	8.35 ± 1.88	13.27 ± 1.60	13.02 ± 1.03	10.84 ± 3.59	17.37 ± 2.05	16.32 ± 0.67	21.01 ± 1.63	20.07 ± 2.33	23.57 ± 3.09	38.36 ± 3.18
Packnet	30.08 ± 2.94	34.96 ± 3.33	38.34 ± 2.81	31.97 ± 0.96	46.02 ± 1.68	29.37 ± 1.37	35.67 ± 1.54	32.23 ± 1.18	33.56 ± 1.50	34.11 ± 1.74
WSN	30.53 ± 2.80	29.63 ± 1.11	33.97 ± 1.49	29.63 ± 2.45	46.77 ± 1.02	36.57 ± 1.11	43.60 ± 0.83	41.67 ± 0.90	41.60 ± 1.31	45.97 ± 2.00
Vanilla Hnet	39.66 ± 4.11	30.17 ± 1.40	39.66 ± 2.07	35.91 ± 2.10	44.19 ± 0.13	33.54 ± 1.85	41.05 ± 2.96	37.95 ± 2.52	34.30 ± 5.30	43.88 ± 2.08
H-embed Hnet*	39.59 ± 3.94	30.40 ± 1.42	40.02 ± 2.45	35.47 ± 2.16	43.92 ± 1.22	35.71 ± 1.89	39.56 ± 2.43	38.10 ± 1.09	34.13 ± 4.08	44.73 ± 2.05

Table 7: **ImageNet.Comparison Experiments, Accuracy Final.** The test accuracy of tasks when finishing learning all CL tasks. The mean value and standard deviation are derived with three times running.

Setting	Method	Type	Task 1	Task 2	Task 3	Task 4	Task 5	Task 6	Task 7	Task 8	Task 9	Task 10	Task 11	
PermutedMNIST	Rand-embed	Final	98.09	97.83	97.58	97.85	97.83	97.48	97.08	97.17	96.86	96.87		
		During	98.07	97.79	97.62	97.85	97.85	97.46	97.09	97.09	97.05	96.82	96.87	
	H-embed	Final	98.11	97.83	97.74	97.71	97.82	97.68	97.11	97.55	97.32	96.66	97.32	
		During	98.07	97.79	97.77	97.73	97.87	97.69	97.19	97.19	97.51	96.65	97.32	
	Vanilla	Final	98.10	97.78	97.79	97.50	97.60	97.46	97.37	97.37	97.17	97.21	96.97	
		During	98.07	97.79	97.83	97.51	97.55	97.46	97.38	97.38	97.14	97.19	96.97	
Cifar10/100	Rand-embed	Final	70.47	71.80	69.10	71.40	64.60	69.10	66.70	72.80	71.30	74.50	81.20	
		During	79.47	76.60	71.90	78.60	75.00	77.00	76.20	76.20	76.00	75.00	77.40	81.20
	H-embed	Final	71.29	75.60	67.60	70.20	68.80	70.20	67.30	67.30	73.20	71.40	77.50	82.10
		During	79.47	76.60	73.80	77.60	75.20	77.90	77.50	77.50	76.70	73.10	78.50	82.10
	Vanilla	Final	70.27	71.70	65.90	69.90	65.70	67.30	64.30	64.30	70.30	69.70	71.00	80.40
		During	79.47	76.60	71.70	78.00	75.80	77.50	76.50	76.50	76.20	75.70	76.50	80.40
ImageNet-R	Rand-embed	Final	39.96	31.98	41.59	35.13	45.00	35.34	39.68	36.01	32.88	42.89		
		During	40.70	31.84	41.95	34.84	44.19	35.34	39.14	39.14	35.53	33.22	42.89	
	H-embed	Final	40.33	32.40	42.86	36.30	45.65	35.97	39.86	39.86	39.47	33.22	46.07	
		During	40.70	31.84	43.04	36.01	45.65	35.97	40.75	40.75	39.31	33.05	46.07	
	Vanilla	Final	40.52	32.12	42.50	35.57	44.19	34.07	41.65	41.65	36.32	31.35	43.74	
		During	40.70	31.84	42.86	35.86	43.71	33.91	42.37	42.37	36.64	31.35	43.74	

Table 8: Ablation Studies, During and Final Accuracy.